Thermally actuated interferometric sensors based on the thermal expansion of transparent elastomeric media

Bartosz A. Grzybowski, Scott T. Brittain, and George M. Whitesides[a)]
Department of Chemistry and Chemical Biology, Harvard University, Cambridge, Massachusetts 02138

(Received 6 October 1998; accepted for publication 13 January 1999)

In this article the fabrication and characterization of two thermally actuated optical devices for the measurement of temperature and power are described. A transparent polymer having a high coefficient of thermal expansion—poly(dimethylsiloxane) (PDMS)—was used as the temperature-sensitive medium. Changes in the dimensions of the polymer on heating caused the observed optical responses of both devices. The temperature sensor based on the Fabry–Pérot cavity measures temperature differences to a precision of 0.005 °C within the linear working ranges of the device. The power sensor uses the architecture of a Mach–Zender interferometer; it is suitable for measurements of powers in the mW/cm^2 range, delivered optically to the surface of the device in the visible wavelength region. The devices are inexpensive, easy to fabricate, and mechanically rugged. They offer alternatives to other sensors for measuring temperature and power. © *1999 American Institute of Physics.* [S0034-6748(99)05004-2]

I. INTRODUCTION

In this article the fabrication and characterization of two thermally actuated interferometric optical devices whose operation hinges on thermal expansion of an optically transparent elastomeric medium—poly(dimethylsiloxane) (PDMS)–that encapsulates the reflective surfaces are described. The first device is a temperature sensor based on a Fabry–Pérot cavity embedded in PDMS. Although many types of devices based on Fabry–Pérot interferometers have been produced,[1–3] that described here is new in its method of transducing temperature into separation of the reflective surfaces of the interferometer. This temperature sensor offers several attractive characteristics: it is easy to fabricate, mechanically durable, and has a resolution of 0.005 °C within its linear working ranges that matches that of good conventional temperature sensors.[4,5] The second system is a micromanufactured power sensor that uses the architecture of the Mach–Zender interferometer to measure power delivered optically (as visible light) to the surface of the device. The interplay between dimensional changes due to thermal expansion and to heat transfer renders this device suitable for power measurements in the mW/cm^2 range.

II. FABRICATION

The Fabry–Pérot temperature sensor was fabricated using a three-step process. A 5 mm thick layer of transparent PDMS was cured in a Petri dish in a well-leveled oven. A 10mm×10mm glass slide supporting a mirrored surface (1.5 nm of titanium and 38 nm of gold; reflectivity $R=75\%$) was placed on the PDMS [Fig. 1(a)]. Another layer (4, 15, or 25 mm thick) of elastomer was cast and cured, and the second mirror (1.5 nm of Ti, 38 nm of Au, $R=75\%$) was placed above the first one. One more layer of PDMS was applied and the curing procedure was repeated. The device was then cut out of the cured polymer in the form of a rectangle with a razor blade. This object was used for temperature measurements.

The power sensor based on the Mach–Zender interferometer used three mirrors embedded in a PDMS layer [Fig. 1(b)]. First, a 5 nm titanium adhesion layer was evaporated onto a Si/SiO_2 wafer. Onto this surface, 80 nm of gold was evaporated. To promote adhesion between the gold and PDMS, a self-assembled monolayer (SAM) was formed from $HS(CH_2)_{14}CH{=}{=}CH_2$ on the surface of the gold[6] by rinsing the surface with a 1 mM solution of the thiol in ethanol. PDMS was spin coated onto this reflective surface at 2200 rpm for 40 s to give a 25 μm thick layer. Titanium (5 nm) followed by gold (20 nm, transmissivity, $T\cong 50\%$) were evaporated onto the PDMS. Again, a SAM was formed from $HS(CH_2)_{14}CH{=}{=}CH_2$ on the surface of the gold, and another 25 μm layer of PDMS was applied. Finally, titanium (5 nm) and silver (100 nm, $R=100\%$) were evaporated onto the PDMS surface (silver was used rather than gold because it is easier to pattern and etch). A pattern of 50 μm lines separated by 50 μm was printed onto the surface of the silver with a solution of $HS(CH_2)_{15}CH_3$ in ethanol using a PDMS stamp.[7,8] Selective etching of the silver not protected by the alkanethiol SAM was accomplished using a ferri/ferrocyanide etchant.[9] This procedure gave 50 μm wide silver lines separated by 50 μm [Figs. 1(b) and 2]. The composition of the etchant was $K_2S_2O_3$ (0.1 M), $K_3Fe(CN)_6$ (0.01 M), and $K_4Fe(CN)_6$ (0.001 M). Caution: *Potassium ferricyanide is light sensitive. The photodecomposed products contain free cyanide. Potassium ferricyanide is also incompatible with acids and releases HCN. Conduct the procedures in a well ventilated hood and avoid prolonged exposure of potassium ferricyanide to light.*

[a)]Electronic mail: gwhitesides@gmwgroup.harvard.edu

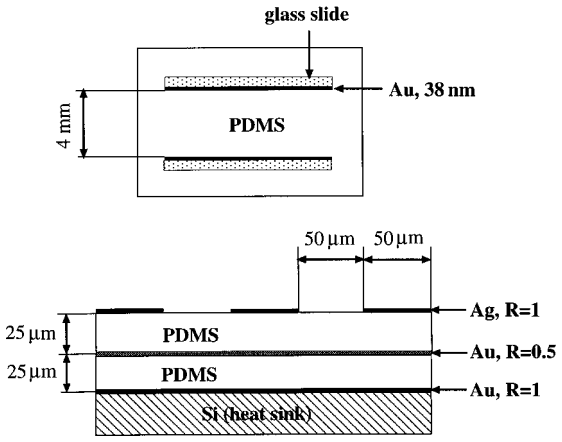

FIG. 1. (a) Fabry–Pérot temperature sensor and (b) the Mach–Zender power sensor.

III. PDMS: TEMPERATURE DEPENDENCE OF THE INDEX OF REFRACTION

In order to determine the temperature dependence of the index of refraction of PDMS, a PDMS prism in the form of an equilateral triangle was fabricated [Fig. 3(a)]. Deflection of a laser beam (HeNe $\lambda = 632.5$ nm) passing through the prism was monitored as a function of temperature. The beam met the surface of the prism at an angle of 45° with respect to the normal, so that at $T_0 = 20\,^{\circ}\mathrm{C}$ it propagated in PDMS almost parallel to the base of the prism ($\gamma_0 = 29.6°$) over the distance of $l = 55$ mm. As the temperature was increased, the beam was deflected by an angle $\gamma(T)$. This deflection resulted in a shift of $\Delta y(T)$ in the position of the laser spot on the screen, placed $L = 4$ m from the prism. Using Snell's law and simple trigonometry, $\Delta y(T)$ could be related to the index of refraction of PDMS $n(T)$ at temperature T by Eq. (1). Figure 3(b) shows the values of $n(T)$ as a function of temperature and the linear regression fit to these data. The slope of the regression line $\beta = -0.000\,10\,^{\circ}\mathrm{C}^{-1}$ and the value of n_0 ($T_0 = 20\,^{\circ}\mathrm{C}$) $= 1.431$, derived by

$$n(T) = \left\{ \sqrt{2} \sin\left[\gamma_0 + \arctan\left(\frac{\sqrt{3}\Delta y(T)}{2(L+1) - \Delta y(T)} \right) \right] \right\}^{-1} \quad (1)$$

fitting the data, were used to obtain the functional dependence of the index of refraction of PDMS on temperature: $n(T) = n(T_0) - \beta(T - T_0)$.

IV. PRINCIPLE OF OPERATION

A. Fabry–Pérot temperature sensor

When a light beam passes through a Fabry–Pérot (FP) cavity in the direction perpendicular to the plane of the mirrors, interference occurs between beams as they reflect multiple times. Let the initial length of the cavity be d_0 (mm), the reflectivity of a single mirror R, and the wavelength of light used in the experiment $\lambda = 632.5$ nm. The length of the cavity is a linear function of temperature $d(T) = d_0 + d_0\alpha(T - T_0)$, where $\alpha = 0.0003\,^{\circ}\mathrm{C}^{-1}$ is the coefficient of thermal expansion of PDMS.[10] Upon one pass through the cavity of length $d(T)$, the phase angle increases by $\Delta\varphi_1$ [Eq. (2)], and, in general, the buildup of phase on m passes is

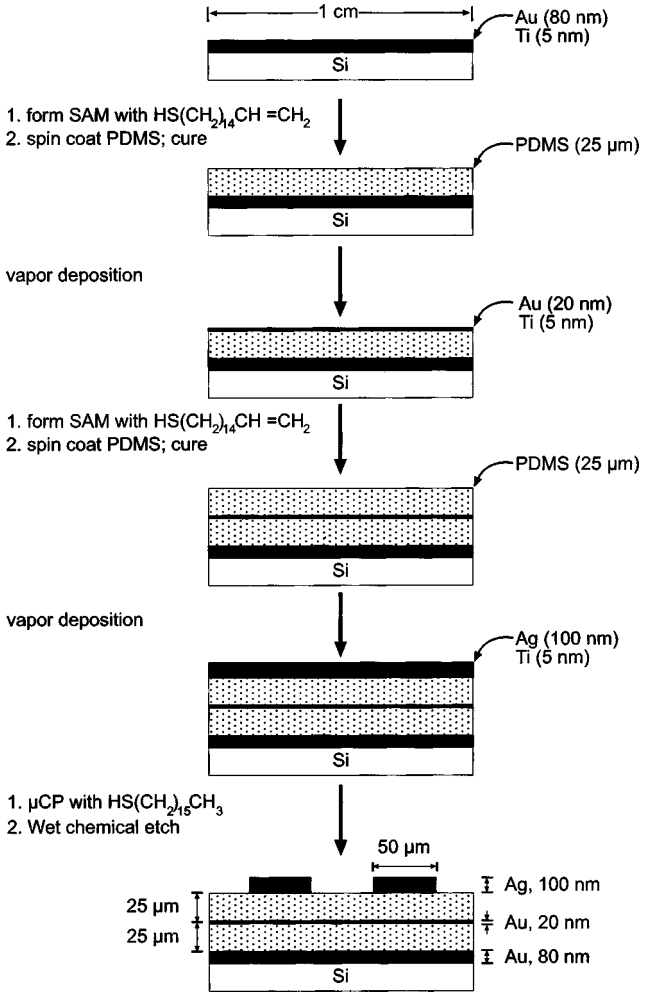

FIG. 2. Fabrication of the Mach–Zender interferometer.

given by Eq. (3). Notice that even when $|\alpha| \approx |\beta|$ (i.e., when the absolute value of the coefficient of thermal expansion is approximately equal to the absolute value of the rate of change of the index of refraction), the increasing

$$\Delta\varphi_1 = \frac{2\pi(n_0 - \beta\Delta T)(d_0 + d_0\alpha\Delta T)}{\lambda} \quad (2)$$

and

$$\Delta\varphi_m = m\,\frac{2\pi(n_0 - \beta\Delta T)(d_0 + d_0\alpha\Delta T)}{\lambda} \quad (3)$$

length of the cavity is not offset by the decreasing index of refraction, and there is still a temperature-dependent buildup of optical phase.

$$\Delta\varphi_m = \frac{2\pi m d_0}{\lambda}(n_0 + (n_0\alpha - \beta)\Delta T - \alpha\beta(\Delta T)^2);$$

$$n_0\alpha - \beta > 0. \quad (4)$$

With the plane wave assumption, and for small absorption of light by the elastomer, we can describe the intensity of transmitted light emerging from the FP cavity by Eq. (5) (I_0 is the intensity of the incident light). Figure 4 shows the periodic behavior of the

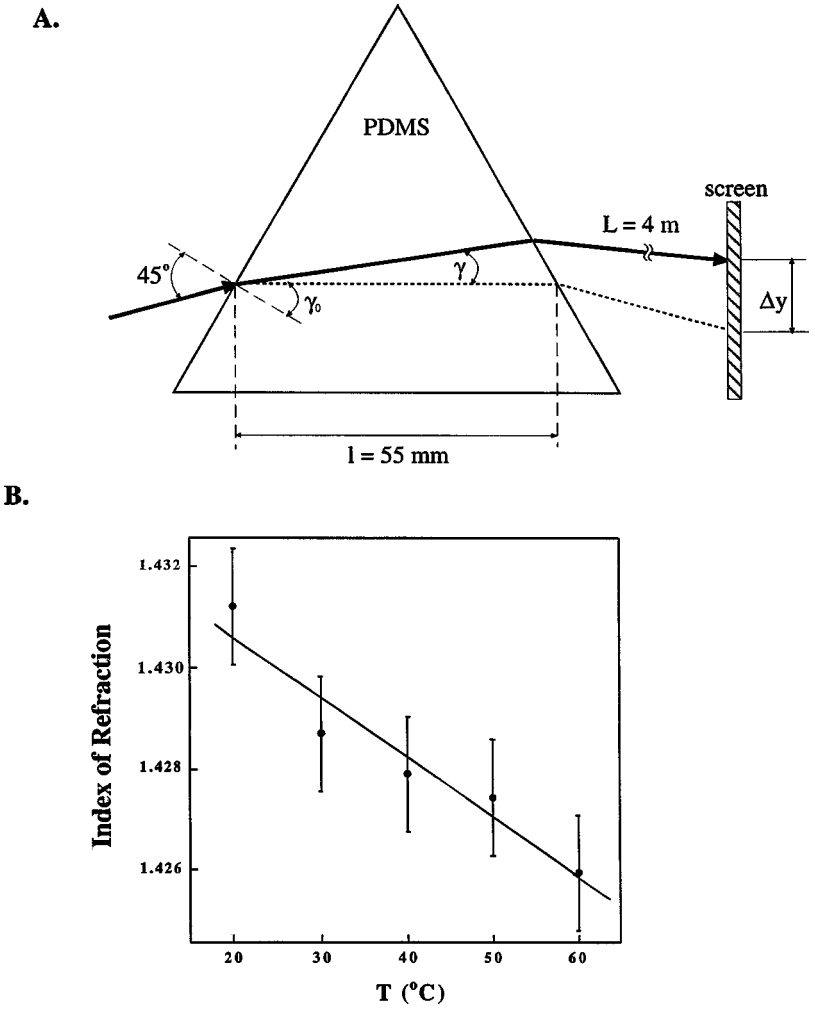

FIG. 3. Measurement of the index of refraction of PDMS as a function of temperature. (a) Drawing illustrating the experimental configuration and (b) drawing giving the calculated values of the index of refraction for temperatures ranging from 20 to 60 °C. The regression line fitted to these data is also shown. The error bars represent standard deviations in two samples and five separate measurements.

$$\frac{I_t}{I_0}=\frac{(1-R)^2}{(1-R)^2+4R\sin^2\left(\dfrac{2\pi(n_0-\beta\Delta T)(d_0+d_0\alpha\Delta T)}{\lambda}\right)} \quad (5)$$

intensity of transmitted light as a function of cavity temperature expected on the basis of Eq. (5). When the intensity of light is at a maximum, Eq. 6(a) holds for all values of m. Similarly, at the minima in light intensity, the relation between the phases is given by

$$\varphi_m-\varphi_{m+2}=2\pi \quad \text{or} \quad (n_0-\beta\Delta T)(d_0+d_0\alpha\Delta T)=\frac{\lambda}{2}, \quad (6a)$$

$$\varphi_m-\varphi_{m+2}=\pi \quad \text{or} \quad (n_0-\beta\Delta T)(d_0+d_0\alpha\Delta T)=\frac{\lambda}{4} \quad (6b)$$

[Eq. (6b)]. Near the resting temperature T_0, the change in temperature $\Delta T(T_0)$ required for the light intensity to go from minimum to maximum (or vice versa) is given by

$$\Delta T(T_0)=\frac{\lambda}{4(n_0\alpha-\beta)d_0} \quad (7)$$

[Eq. (7)]. In our device with cavity length $d_0=4.0\,\text{mm}$, $\Delta T_0\approx 0.12\,^\circ\text{C}$. At higher temperatures, $\Delta T(T)$ can be approximated by Eq. (8). For PDMS this change in

$$\frac{\Delta T(T)}{\Delta T(T_0)}\approx\frac{(n_0\alpha-\beta)}{(n_0\alpha-\beta)-\alpha(T-T_0)(n_0\alpha-2\beta)} \quad (8)$$

periodicity is negligible (<1%) over the working range of the device (20–60 °C).

B. Mach–Zender power sensor

The second device employs the architecture of a Mach–Zender interferometer (Fig. 5).[5] The laser beam (λ

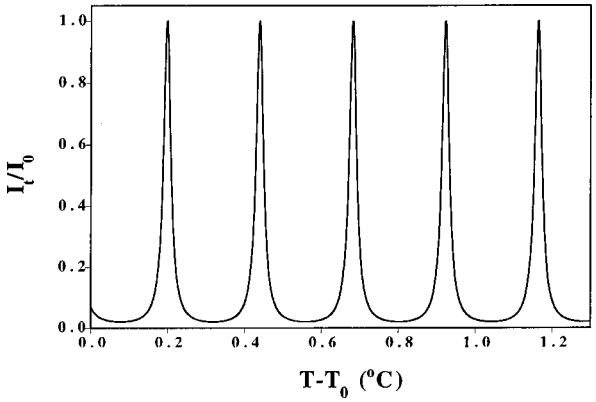

FIG. 4. Calculated intensity of the transmitted light (λ=632.5 nm) as a function of temperature increase for the Fabry–Pérot temperature sensor. The reflectivity assumed for the mirrors was 75% and the initial length of the cavity was 4.000 mm.

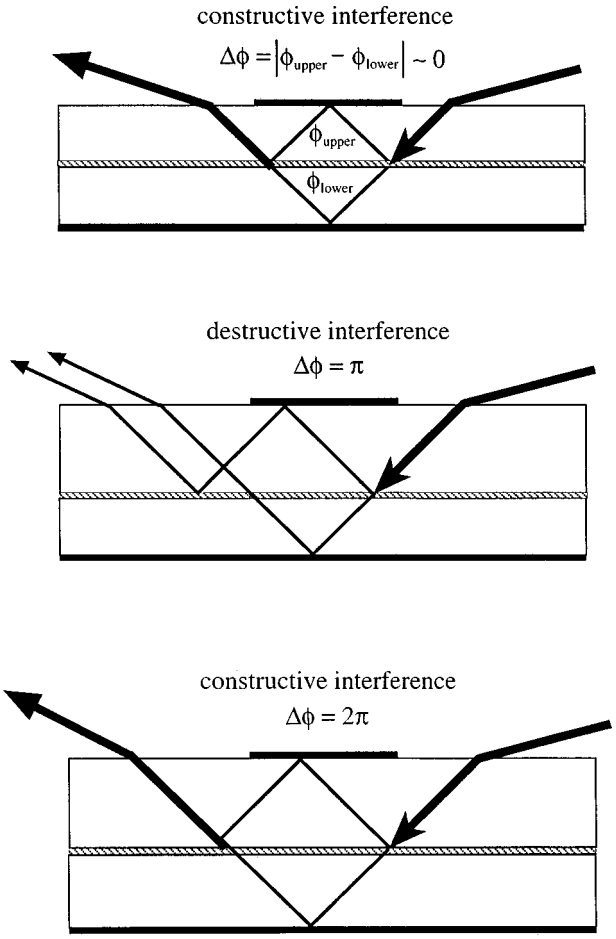

FIG. 5. Principle of operation of the Mach–Zender power sensor. In the resting state (top picture), the top and bottom beams travel approximately equal optical paths and interfere constructively on the surface of the middle gold mirror. When heat is delivered to the top of the device, the upper layer of the PDMS expands more rapidly than the lower (middle picture), and the optical paths traveled by the top and bottom beams are different. If the difference in optical paths, $\Delta\phi$, is equal to π (or its odd multiple), destructive interference occurs (middle picture), and the intensity of the laser beam reflected from the device drops. If $\Delta\phi = 2n\pi$, $n = 0,1,2,...$, the beams interfere constructively and the intensity of the laser beam is maximal (bottom picture).

$=632.5$ nm, ~ 1 mW/mm^2) meets the surface of the device at an angle of $\sim 80°$ with respect to the normal, and propagates in the PDMS at an angle of 45° with respect to the normal. At the middle, semitransparent layer of gold ($T \sim 50\%$) it splits into two beams, a top and a bottom, that subsequently reflect from the silver surface mirror and the gold bottom mirror (both with $R = 100\%$). When the device is in the resting state, the top and the bottom beams travel optical paths of approximately equal lengths, so when they later combine at the surface of the middle gold layer, they are in phase and interfere constructively.

Uniform illumination of the top surface of the device with the laser beam ($\lambda = 632.5$ nm) creates a temperature gradient in the direction perpendicular to the silicon wafer. Heating occurs by adsorption of light by the silver grating on the surface: this structure adsorbs light and transfers the resulting heat to the PDMS by diffusion. The increase in temperature increases the thicknesses of the PDMS layers. We performed qualitative heat flow calculations for the system

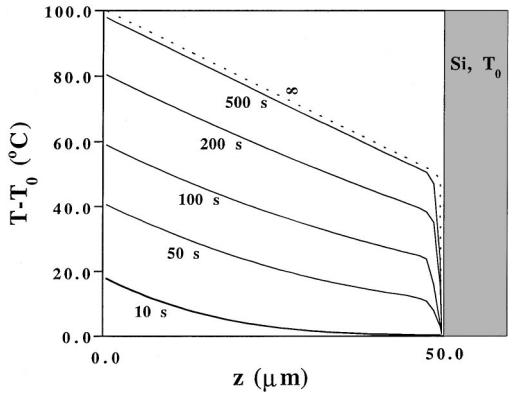

FIG. 6. Temperature profiles along the z axis (perpendicular to the plane of the silicon wafer) for the Mach–Zender interferometer. The curves describe the evolution of the temperature gradient inside the device for times ranging from 0.1 to 10^3 s. Near the PDMS/silicon wafer interface the temperature profiles are qualitative. The thickness of two PDMS layers is 50 μm. Zero of the z axis corresponds to the PDMS/air interface. At time $t = 0$ the device is at uniform temperature T_0. The temperature inside the device during heating is described by $T(z,t)$ and is a function of both position z and time t. The values of thermodynamic quantities used in the calculations were $Nu = 1.0$, $P = 0.01$, and $qL/K = 50.0$ (see the Appendix for the definitions of these quantities).

(see the Appendix and Fig. 6) to investigate the temporal evolution of temperature profiles. At small times, the upper layer of PDMS (that between the silver lines and the semitransparent gold mirror) heats and expands first. This differential expansion creates a difference in the optical paths, $\Delta\varphi$, traveled by the split beams: the upper optical path is now longer. As the result of this change in optical paths, the intensity of the laser beam reflected from the device (after interference between the beam propagating only in the upper layer of PDMS and that propagating in the lower layer) changes [Fig. 7(a)]. When $\Delta\varphi = m\pi$ ($m = 1,3,5,...$), destructive interference occurs and the intensity is at a minimum, and when $\Delta\varphi = 2m\pi$ ($m = 1,2,3,...$), the split beams interfere constructively and maximal intensity is observed. If the power is delivered continuously, heat diffusion equalizes the temperature differences in the PDMS layers.[11] The period of oscillation of the intensity of the reflected laser beam increases and, when the device comes to thermal equilibrium at large times, no changes in the intensity are observed [Fig. 7(b)].

If the intensity of the laser beam is low (<1 mW/cm^2), so that it delivers a negligible amount of heat to the device, it can be used as a probing beam while heat is delivered by some other light source. With intense sources of radiation (~ 100 mW/cm^2), the intensity of the probing laser beam oscillates as described before. When, however, the delivered power is low (<10 mW/cm^2), heat diffusion quickly smoothes the temperature profiles across the device, and only one period of oscillation in the intensity of the probing beam is observed before thermal equilibrium across the device is established. The intensity initially decays, reaches the minimum, and then slowly increases to its original value (Fig. 9).

The depth of the minimum in the intensity of the reflected laser beam is proportional to the power delivered to the device. For very small powers (<1 mW/cm^2), the change in the temperature of the surface (silver lines) is very small;

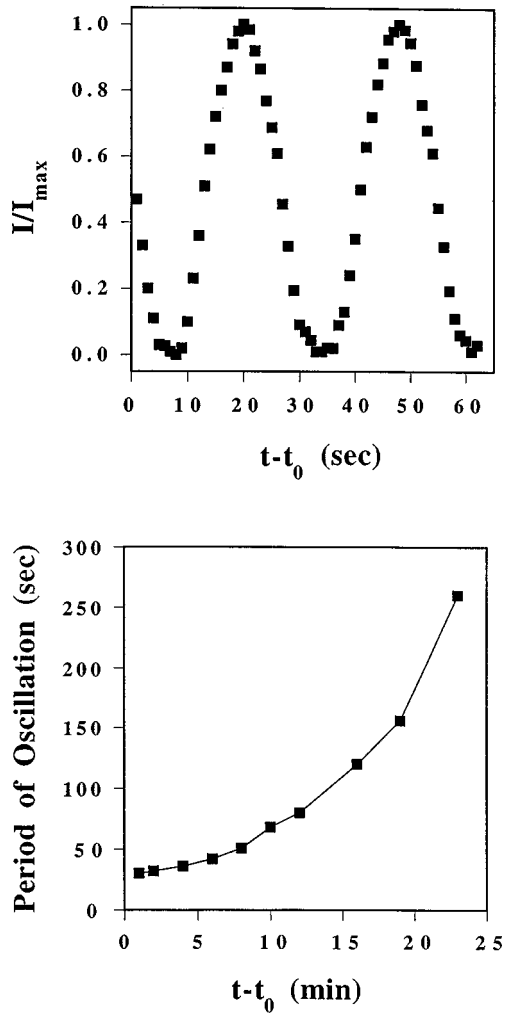

FIG. 7. (a) Modulation of the intensity of the laser beam reflected from the Mach–Zender interferometer. The beam ($\lambda=632.5$ nm, 1 mW/mm^2) met the surface at an angle of $\sim 80°$ with respect to the normal; the surface was illuminated uniformly. (b) Dependence of the period of the modulation of the intensity as a function of time. The period increases as the device reaches thermal equilibrium.

the temperature profiles across the device are flattened by heat diffusion, and no minimum is observed.

V. RESULTS AND DISCUSSION

A. Fabry–Pérot temperature sensor

Figure 8 shows the measured dependence of the intensity of the probing laser beam as a function of the temperature (as measured by an internal thermocouple) of the FP device with a 4.0 mm cavity. The consecutive extrema occur in intervals of 0.115 °C, in good agreement with the value of 0.12 °C estimated from the dimensions of the cavity and from the values of the coefficient of thermal expansion and the index of refraction. Near the intensity minima the temperature changes can be measured to an accuracy of 0.05 °C, and in the regions of linear intensity-temperature dependence the precision of temperature measurement improves markedly to 0.005 °C. The measured contrast ratio (intensity at a maximum to intensity at a minimum) is 10.5 (10.2 dB). The device gave stable readings over a 30 °C range from 20.4 to

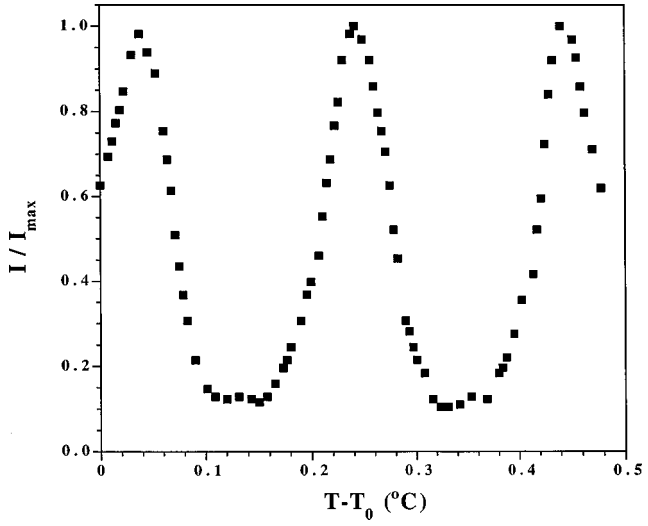

FIG. 8. Intensity of the transmitted light ($\lambda=632.5$ nm) as a function of temperature for the Fabry–Pérot thermal sensor. The length of the cavity was 4.0 mm and the reflectivity of the mirrors was 75%.

50.4 °C. Above this limit, the amplitude of intensity of oscillation decays, probably due to nonuniformities in the expansion of the polymer, and resultant misalignment of the mirrors. The device operated equally well in the forward (heating) and reverse (cooling) modes.

As higher temperature sensitivity is expected for longer cavities, we fabricated two more devices—one having a cavity length of 15 mm, the other 25 mm. The performance of both was much worse than that with the 4 mm cavity: when the length of the cavity was extended, even a small misalignment of the mirrors resulted in large angular deflection of the multiple-reflection beams. Interference no longer took place and the intensity of the monitored laser beam dropped abruptly. In addition, the large dimensions made uniform heating of those devices difficult.

Because this sensor is contained within an elastomeric polymer matrix, it is extremely durable. It is resistant to most chemicals (dipping in gold etchant for 5 min did not destroy the device), as well as to mechanical stresses (the device was dropped on the floor and thrown against the wall without damage). The response of the device was stable over many heating–cooling cycles (more than 100), and did not change over the period of several months.

B. Mach–Zender power sensor

With the laser beam used simultaneously for heating and probing, the intensity of the reflected beam oscillated periodically as described in Sec. IV B: the initial period was 28 s and it increased with time as the thermal equilibrium across the device was being established (Fig. 7). The measured contrast ratios were ~ 25 dB. After ~ 45 min, no changes in the intensity of the reflected beam were observed.

When a low power laser ($\lambda=632.5$ nm, ~ 0.5 mW/cm^2) was used for probing only and heat was delivered from another light source (a fiber optic illuminator), powers of the illuminating source below 10 mW/cm^2 were measured. Figure 9 shows the response of the Mach–Zender sensor to illumination with white light of power of 7 mW/cm^2. Within

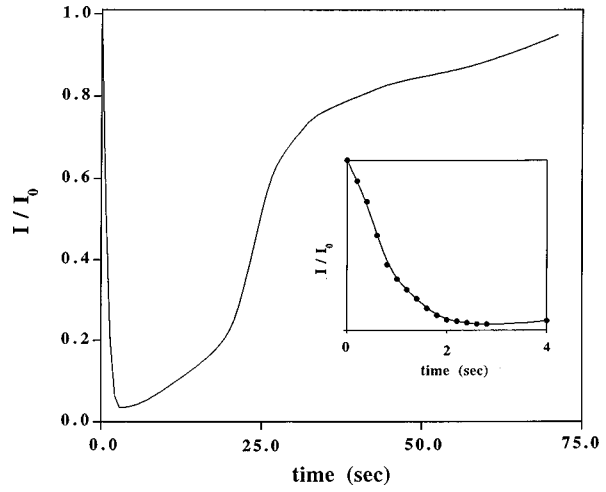

FIG. 9. Dependence of the intensity of a probing laser beam ($\lambda=632.5$ nm, 0.5 mW/cm^2) reflected from the Mach–Zender interferometer as a function of time. The device was illuminated uniformly with white light of power of 7 mW/cm^2. The inset shows the decrease in the intensity of the probing beam during the first 3 s.

the first 3 s, the intensity of the reflected interference beam dropped by a factor of 20. As the device was heated further, the initial intensity recovered within ~70 s. As the power of the illuminating light was varied, the depth of the intensity minimum changed (Fig. 10): when the intensity was lowered, the depth of the minimum decreased. Below ~1 mW/cm^2, a minimum in intensity was not observed at all, since heat diffusion was faster than the rate at which energy is delivered to the system. By measuring the depth of the intensity minimum, the power of an illuminating source could be assessed (Fig. 10).

The Mach–Zender device described here can, in principle, be used for power measurements at powers other than the mW/cm^2 range examined here. Choosing an elastomer with a lower coefficient of thermal expansion will render the system suitable for measurements of higher power. Because the spin-coating procedure by which PDMS layers were applied ensures excellent surface flatness, alignment of the mirrors is not an issue. The differences in the optical responses of nominally identical devices (three copies were fabricated) did not excede 10%; the devices gave stable readings over more than 50 heating–cooling cycles, and over the period of several months.

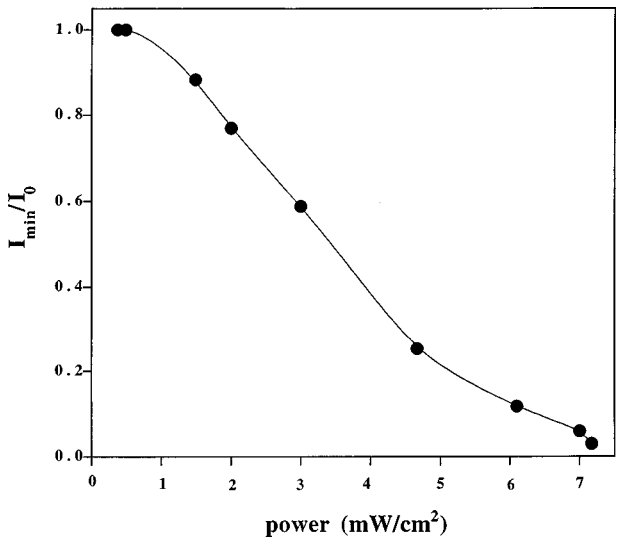

FIG. 10. Response of the Mach–Zender power sensor to illumination with low-power visible light. The depths of the minima in the intensity of the reflected probing laser beam decreased as the power of the illuminating radiation decreased. For powers less than ~1 mW/cm^2, no minimum was observed.

VI. EXPERIMENT

A. Fabry–Pérot temperature sensor

The PDMS prepolymer and curing agent were purchased from Dow Corning. A 1:10 mixture of curing agent and prepolymer was used to fabricate the device. The mixture was cured thermally at 60 °C for 2 h. A HeNe laser ($\lambda=632$ nm) was used as a probe beam. The FP device was mounted so that this laser beam propagated in the PDMS perpendicular to the mirrors. A thermocouple (Omega, DP 462) was placed inside the PDMS to measure the temperature. Heat was delivered to the device by illuminating it uniformly with three fiber optic illuminators (Dolan–Jenner, model 190). The intensity of the outgoing laser beam was monitored with a photodiode (Newport, 1830-C) connected to an oscilloscope.

B. Mach–Zender power sensor

The laser beam (HeNe, $\lambda=632.5$ nm, ~1 mW/mm^2) used for heating and readout met the surface of the device at an angle of 80° with respect to the normal to the plane. Changes in the intensity of the beam were monitored using a silicon photodiode. When the laser beam was used only for readout, its intensity was reduced to ~0.5 mW/cm^2 by passing it through a 0.5% neutral density filter. Heating was then achieved by illuminating the surface of the device uniformly with visible light from a fiber optic illuminator (Dolan-Jenner, model 190). The power output of the fiber optic illuminator was calibrated using a power meter (Thor Labs, S20MM).

To measure the absorptivity of silver grating lines, a HeNe laser ($\lambda=632.5$ nm) was used as a light source. The intensity of light reflected from the device was measured. The reflected light was focused by a biconvex lens placed close to the surface of the device to ensure that the decrease in intensity is not due to scattering of light by the grating. Next, the grating was removed by chemical etching and the absorptivity of the remaining structure (the two PDMS layers and the inner gold mirrors) was assessed in a similar way. The difference in absorptivities from these two measurements gave the value of the absorptivity of the grating.

C. Measurement of the index of refraction of PDMS

To calculate the index of refraction of PDMS, an equilateral PDMS prism was fabricated by casting PDMS against an equilateral master built from three microscope slides. The prism was mounted on a rotational stage (precision of 1/60°) and oriented such that the laser beam (HeNe, $\lambda=632.5$ nm) met the surface of the prism at an angle of 45°. By monitor-

ing the deflection of a laser beam upon passage through the prism, the index of refraction was calculated for temperatures ranging from 20 to 60 °C.

ACKNOWLEDGMENTS

This work was supported by the Defense Advanced Research Project Agency (DARPA), and by the National Science Foundation (NSF) under Award No. ECS-9729405. The authors thank Ned Bowden for helpful discussions.

APPENDIX

Radiation from the illuminating source delivers heat to the system. We verified experimentally that the absorptivity of the top silver layer (~45%) is much higher than that of the rest of the device (that is, PDMS layers and inner gold mirrors which have total absorptivity of ~7%.[12] On the basis of this observation, we assumed that the heat transfer proceeds from the top silver layer to the bulk of the device. We treated the device as a uniform slab of PDMS of thickness $L=50\ \mu$m, subjected to a heat input at a constant rate q into one face ($z=0$; zero of the z axis corresponds to the PDMS/air interface, and the axis is perpendicular to surface of the device), while the other face ($z=L$; PDMS/silicon wafer interface) is in contact with a semi-infinite medium (silicon) at constant temperature T_0. At time $t=0$ the system is at a uniform temperature T_0. The heat equation for this system plate was solved.[13] The pertinent equations and boundary conditions are given below (K stands for thermal conductivity of PDMS; C is its heat capacity, and ρ denotes the density of PDMS):

(1) $\partial T(z,t)/\partial t = K(\partial^2 T(z,t)/\partial z^2)$, general equation of heat diffusion;
(2) $q=-K(\partial T(0,t)/\partial z)$, the rate of heat input across the $z=0$ surface is equal to q;
(3) $h[T(L,t)-T_0]=-K(\partial T(L,t)/\partial z)$, the rate of heat flow across the PDMS/silicon interface is proportional to the temperature difference between the $z=L$ surface of PDMS and the temperature of the silicon wafer T_0.
(4) $\int_0^L (T(z,t)-T_0)C\rho dz = qt-\int_0^t h(T(L,t)-T_0)dt$, the total gain in heat content by PDMS at any time is equal to the difference between the total heat input and output up to that time.

The solution to this problem is given by[13]

$$T(z,t)=T_0+\frac{qL}{K}\left[1-\frac{z}{L}+\frac{1}{Nu}-F\left(\frac{z}{L},P\right)\right],$$

where Nu is a modified Nusselt number $Nu=hL/K$, P is a dimensionless quantity equal to $Kt/CL^2\rho$, and $F[(z/L),P]=2$;

$$\sum_{n=1}^{\infty}\beta_n^{-2}A_n\cos\left(\frac{z\beta_n}{L}\right)\exp(-\beta_n^2 P),$$

in which β_n is defined by $\cot\beta=\beta/Nu$, and $A_n=(\beta_n^2+Nu^2)/(\beta_n^2+Nu(1+Nu))$. The temperature profiles in Fig. 6 were generated using these equations; within a very thin boundary layer the (PDMS/silicon wafer interface) they were adjusted to ensure the finitness of temperature gradient.[14]

[1] J. Peerlings, A. Dehe, A. Vogt, M. Tilsch, C. Hebeler, and F. Langenhan, IEEE Photonics Technol. Lett. **9**, 1235 (1997).
[2] E. C. Vail, M. S. Wu, G. S. Li, L. Eng, and C. J. Chang-Hasnain, Electron. Lett. **2**, 228 (1995).
[3] A. T. Tran, Y. H. Lo, Z. H. Zhu, D. Haronian, and E. Mozdy, IEEE Photonics Technol. Lett. **8**, 393 (1996).
[4] Y. Rao, D. J. Webb, D. A. Jackson, L. Zhang, and I. Bennion, J. Lightwave Technol. **15**, 779 (1997).
[5] M. Born and E. Wolf, *Principles of Optics* (Pergamon, Oxford, 1980).
[6] This SAM improves adhesion between the gold and PDMS layers through reaction of the terminal vinyl group with the liquid prepolymer during crosslinking.
[7] J. L. Wilbur, A. Kumar, E. Kim, and G. M. Whitesides, Adv. Mater. **6**, 600 (1994).
[8] For a general review on soft lithography and microcontact printing see, for example, Y. Xia and G. M. Whitesides, Angew. Chem. Int. Ed. Engl. **37**, 551 (1998).
[9] Y. Xia, X.-M. Zhao, E. Kim, and G. M. Whitesides, Chem. Mater. **7**, 2332 (1995).
[10] O. J. Schueller, D. C. Duffy, J. A. Rogers, S. T. Brittain, and G. M. Whitesides, Sens. Actuators (in press); Dow Corning, Sylgard® 184 technical specification sheet.
[11] The high thermal conductivity of the thin gold interfacial layer allows heat to diffuse into the lower PDMS layer.
[12] After HF etching and subsequent exposure to air, the top silver layer is corrugated and oxidized; both factors contribute to its high absorptivity.
[13] A. B. Newman and L. Green, Trans. Electrochem. Soc. **66**, 345 (1934); H. S. Carslaw and J. C. Jaeger, *Conduction of Heat in Solids* (Oxford University Press, London, 1959), p. 125.
[14] The assumption of constant surface coefficient of heat transfer h leads to discontinuity in calculated temperature profiles at $z=L$. In reality, h is a function of many variables specific to the heat flow across the interface. The determination of the functional form of h is beyond the scope of this article, however. For more thorough discussion see, for example, M. Jakob, *Heat Transfer* (Wiley, New York, 1949), pp. 12–22.